

Article

A Parasitic Resonator-Based Diamond-Shaped Microstrip Antenna for Microwave Imaging Applications

Md Zulfiker Mahmud ^{1,2,*}, Md Tarikul. Islam ^{1,*}, Ali F. Almutairi ^{3,*}, Md Samsuzzaman ¹, U.K. Acharjee ⁴ and Mohammad Tariqul Islam ^{1,*}

¹ Faculty of Engineering and Built Environment, Universiti Kebangsaan Malaysia, Bangi 43600 UKM, Selangor, Malaysia; samsuzzaman@ukm.edu.my

² Department of AIS, Jagannath University, Dhaka 1100, Bangladesh

³ Electrical Engineering Department, Kuwait University, Safat 13060, Kuwait

⁴ Department of CSE, Jagannath University, Dhaka 1100, Bangladesh; uzal@cse.jnu.ac.bd

* Correspondence: zulfikerm@yahoo.com (M.Z.M.); p94299@siswa.ukm.edu.my (Md.T.I.); ali.almut@ku.edu.kw (A.F.A.); tariqul@ukm.edu.my (M.T.I.); Tel.: +60-198107953 (Md.T.I.)

Received: 10 February 2019; Accepted: 9 April 2019; Published: 16 April 2019



Abstract: This study proposes a new parasitic resonator-based diamond-shaped microstrip patch antenna for ultra-wideband microwave imaging applications. The antenna consists of a diamond-shaped radiating patch, partial ground plane, and four-star shape parasitic elements. The use of parasitic elements improves the antenna performance in terms of the bandwidth and gain. The proposed prototype has a compact dimension of $30 \times 25 \times 1.6 \text{ mm}^3$. The antenna achieves an overall bandwidth ($S_{11} < -10\text{dB}$) of 7.6 GHz (2.7–10.3 GHz) with more than 4 dBi realized gain and 80% efficiency across the radiating bandwidth. The modified structures of the design extended the usable upper frequency from 9.7 GHz to 10.3 GHz, and the lower frequency is decreased from 3.4 GHz to 2.7 GHz with maintaining the omnidirectional radiation pattern. The design and simulation of the antenna are performed in the 3D electromagnetic simulator CST Microwave Studio. The proposed antenna is used for breast phantom measurement system to analyze the variation of backscattering signal and transmit-received pulses. The observation during the analysis of the numerical and measured data reveals that the designed antenna is a suitable candidate for ultra-wideband (UWB)-based microwave imaging applications.

Keywords: microwave imaging; UWB; parasitic element; resonator; microstrip antenna

1. Introduction

In microwave imaging (MWI), the radiating backscattered signals from the target region of the human body are collected and analyzed to retrieve the changes of electrical properties inside the tissues. Malignant cells present a higher dielectric constant due to high water content. The changes in backscattered signals that reflect the variances of electrical properties predict the presence of tumorous cells. The principle of this technology is that microwaves travel through the human body from the transmitting antenna and are collected by the receiving antenna. A change is found in the traveling signals through the region-of-interest (ROI). In such a condition, the incident waves are scattered which have strong effects on the amount of incident wave energy at the receiver end. In a MWI system, microstrip antennas are acting as a transceiver. Naturally, two different categories of antennas are mostly used in MWI systems: firstly, the resonance-type antennas, and the traveling waves antennas such as Vivaldi. An ultra-wideband antenna (UWB) is capable of operating in both high and low-frequency bands, with some extraordinary properties like contactless remote operations,

environmental friendliness, biocompatibility, intrinsic electrical transducers, and biological friendliness. These unique features create a great interest to researchers using UWB antennas for medical applications. Numerous types of UWB antennas are proposed for MWI applications: directional vs. omnidirectional radiation patterns; high vs. low frequency; wide ranges vs. narrow bands, etc. The requirement of antennas for a MWI system is to be smaller in size along with higher gain and higher efficiency, with highly well-matched penetration to human tissue.

Several UWB antennas have been reported for use in MWI applications in the past few years. In [1] Jianli et al. surveyed UWB antennas for MWI applications and recommended some required features which include: lower energy consumption; capability to penetrate objects; multipath resolving capacity or higher precision range and lower electromagnetic radiation (-41.3 dB). To achieve the required features, researchers have proposed a quantity of UWB antennas such as: planar square monopole [2]; V-shaped monopole [3]; metamaterial-based UWB [4]; hook-shaped UWB; a monopole antenna by Liu and Yang is presented in [5] operating from 3 GHz to 10.7 GHz with a dimension of $10 \times 10 \times 1.6$ mm³; semi-circular [6]; UWB [7,8]; square patch [9]; flexible CPW-fed fishtail [10]; tapered slot [11]; several types of Vivaldi antennas [12,13]; and many others. UWB antennas properties can be increased by modifying the shape of the radiator like circular, rectangular, elliptical, heart shape, etc. and the ground structure, and can achieve wide bandwidth [14–17]. A compact size UWB antenna with a heart shape using triangular patches is proposed operating from 4 GHz to 19.1 GHz with dimensions of $25 \times 26 \times 0.5$ mm³ [18]. An ultra-wideband monopole antenna with inverted T-shaped notch in the ground plane, operating from 3.12 GHz to 12.73 GHz, is presented with a compact size of 12×18 mm² [2]. A tapered-shaped slot antenna [11] with areas of 22×24 mm² presented operation frequencies from 3 GHz to 11.2 GHz. UWB antennas have begun to be used for MWI in the last decade. Analysts speculated that MWI could be utilized to separate typical and cancerous tissues regarding the electrical properties, permittivity, dielectric constant and conductivity. The value of the dielectric constant of the tumorous tissue is assessed to be five to 10 times higher than the typical tissues [19] because of malignant tissues having a higher water content [20,21] than healthy tissues or fat [22]. In recent years, UWB communication has been attractive to a wireless communication system for its special features like extensive high data transmission rate, low spectral power density, and low interference. A number of the techniques are proposed by several researchers to enhance the performance of UWB antenna such as using a metamaterials layer [4], defected ground plane [23], modified pattern of patch [24], adding an extra slot or super-state, and many more. It is still a challenge to design a proficient compact UWB antenna. A tapered-shape slot antenna for UWB application with an overall dimension of 22×24 mm² and CPW antenna with a dimension of $25 \times 25 \times 1.6$ mm³ for achieving UWB bands was also proposed [11,25].

In this study, a new parasitic resonator-based diamond-shaped patch antenna for ultra-wideband microwave imaging applications is proposed. The parasitic element is used to improve the performance with the desired properties for UWB-based microwave imaging applications. The proposed antenna is also used for a breast phantom measurement system to analyze the variation of the backscattering signal and transmit-received pulses.

2. Antenna Design

The geometric layout of the proposed antenna is shown in Figure 1. The proposed antenna is designed on Rogers RT/Duroid 5880 substrate material having 2.2 dielectric constant and 0.0009 loss tangent. The antenna is designed with a diamond-shaped patch, partial ground plane and star-shaped parasitic elements on the substrate. The diamond-shaped patch with incremental staircase design is used as a main radiating element of the antenna. The overall dimension of the antenna is $30 \times 25 \times 1.6$ mm³. The height and width of the ground plane are 6.5 mm and 24 mm. The feedline is 3.0 mm in width and 8.0 mm in height. The feedline is directly connected to the diamond-shaped patch. The designed antenna is fed by a 50 Ω microstrip line. Three parasitic elements are positioned above the ground plane, and another one is placed beside the feedline.

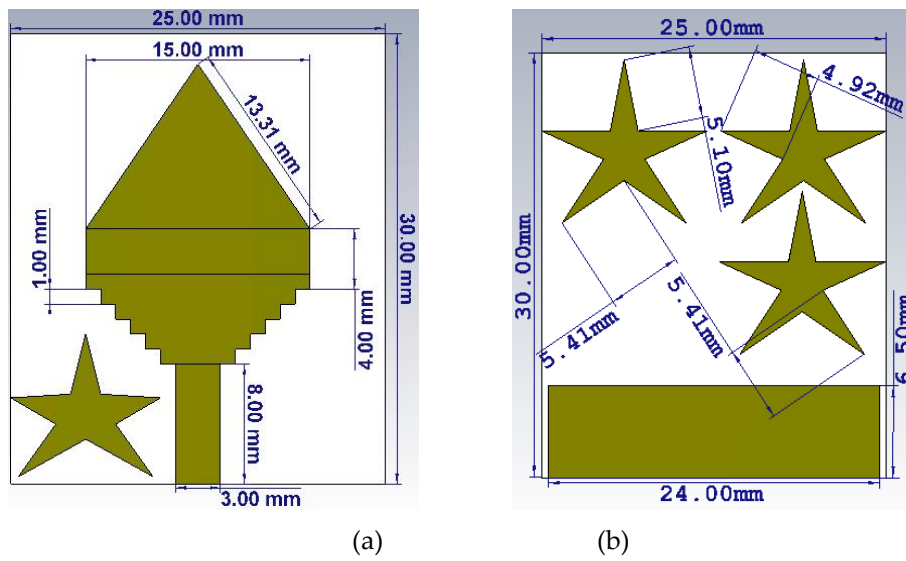


Figure 1. Geometric structure of the realized antenna: (a) front view and (b) back view.

The existence of parasitic elements and staircase diamond shape of the patch and optimum ground plane has a strong effect for the impedance matching. By adding the star-shaped parasitic elements, the side lobe level is simultaneously reducing, and gain in the main lobe is increased and corrects the squint effects which provides improvements in radiation characteristics. The parasitic elements promote the main radiator optimal conditions to avoid the trapping. Slot edges improve the radiation characteristics due to the control of surface current distribution near the lateral antenna edges. Figure 2 presents the effect of the parasitic resonator on the reflection coefficient. It shows that the parasitic resonator has a strong effect both in lower and upper bandwidth enhancement. The modified structures by using resonator and staircase patch extended the usable upper frequency by about 600 MHz (shifted from 9.7 to 10.3 GHz), and the lower frequency is decreased by about 700 MHz (shifted from 3.4 to 2.7 GHz). The gain of the antenna for the different structure is portrayed in Figure 3. The figure concluded that the gain is higher for proposed configuration than others. The peak gain reached 6 dBi from 4 dBi by using the parasitic resonators. The use of parasitic elements creates some extra current conducting paths. This structure changes the capacitance and inductance of the input impedance of the prototype, which leads to changes in the antenna characteristics.

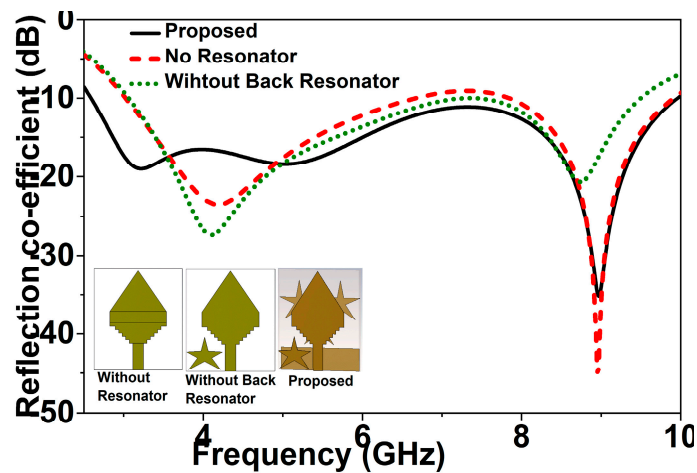


Figure 2. Effects of the parasitic resonator on reflection coefficient.

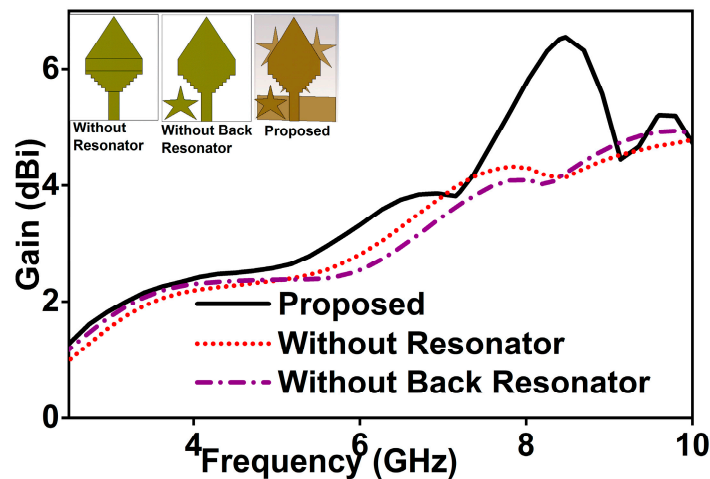


Figure 3. Effects of the parasitic resonator to the gain of the antenna.

3. Results and Discussion

The fabricated prototype of the antenna is shown in Figure 4. The measured reflection coefficient and far field results were achieved using the Agilent performance network analyzer (10 MHz–67 GHz) and UKM Satimo near field StarLab, respectively. The UKM Satimo StarLab near-field antenna measurement system has the measurement chamber fitted with the equipments from the Microwave Vision Group (MVG) to measure the radiation pattern, efficiency, and gain of the prototype. The system has the facility to measure the electric fields of the antenna in the near field region for computing the equivalent far-field values of the antenna under test (AUT). The AUT is positioned on the middle of a circular “arch” and placed on the test bed which consists of 16 separate receiving antennas. The antennas are placed in a circle with maintaining the same distance. The AUT is rotated 360° horizontally, and this turning and array antennas make a full 3D scan. After taking the near field data, it is now converted to far field data through SatEnv software. Then radiation pattern, gain, and efficiency are computed from the far field data by using the SatEnv software. The simulated and measured reflection coefficient of the realized diamond-shaped antenna is depicted in Figure 5a. The antenna achieves -10dB impedance bandwidth of 7.6 GHz (2.7 GHz–10.3 GHz). The coverage of large bandwidth made the antenna suitable for the multiband application and microwave imaging applications. There were two resonance frequencies wherein the -25 dB impedance was a lower and -35 dB impedance was a higher resonance. The measured efficiency and gain of the proposed prototype are presented in a double Y graph in Figure 5b. The result reveals that the antenna maintains a more than 4 dBi gain over the entire band with a maximum realized gain of 6.2 dBi. Higher gain made the antenna a suitable candidate for the use of UWB applications where high gain is required. The efficiency of the proposed antenna is more than 80% over the bandwidth which confirms its application for high-performance devices. The overall efficiency over the frequency is presented in Figure 5b. It is observed that the use of modified structure including a parasitic resonator on substrate and staircase diamond shape patch creates few extra excitations, and hence the operating bandwidth is increased.

The numerical surface current distribution of the realized antenna is presented in Figure 6a,b for two resonant frequency of 5.0 GHz and 9.47 GHz. CST microwave simulation tools are used for observing surface current. The most dominant surface current conducting area of the proposed prototype is around the fed line and lower part of the patch. At higher frequency there exist few nulls on the patch because of the higher order current mode. The existence of the parasitic element changes the current conducting path and changes the antenna characteristics specially to extend the upper limit of the operating frequency band. The proposed antenna maintains the harmonic order flow in both patch and ground plane which assists in obtaining the wide frequency bandwidth.

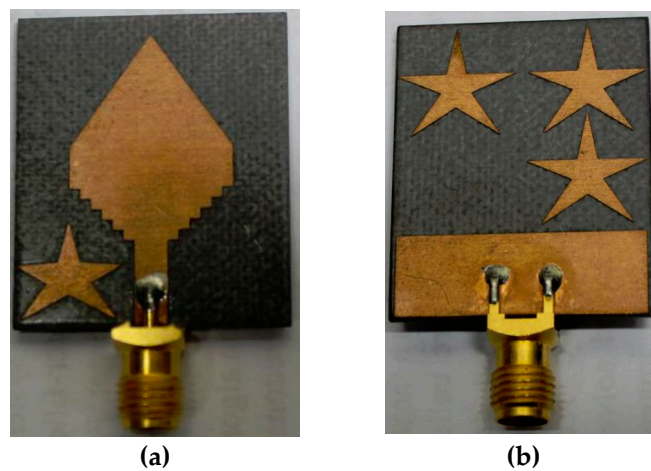


Figure 4. The fabricated prototype: (a) front side (b) back side.

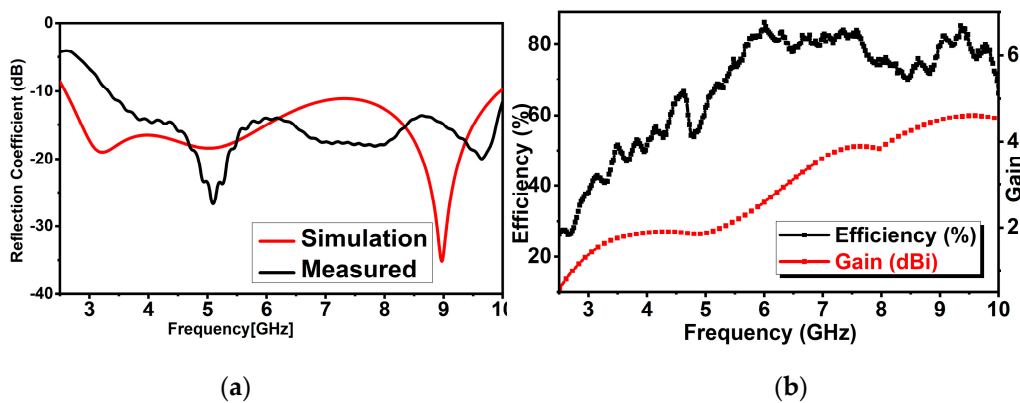


Figure 5. (a) Reflection coefficient (S_{11}). (b) Peak gain and efficiency (measured).

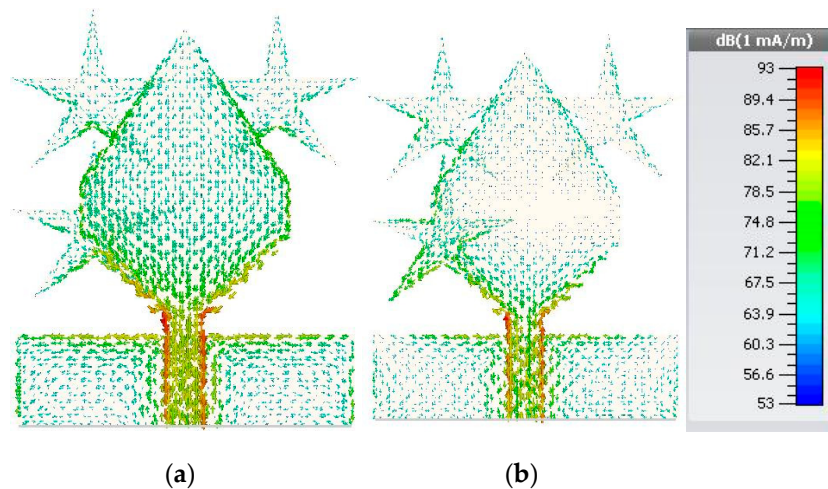


Figure 6. The simulated vector current distribution at: (a) 5 GHz and (b) 9.47 GHz.

The front to front time-domain performance of the antenna is presented in Figure 7 at the distance of 200 mm. The transmitted and received pulses are almost the same except it spread slightly. This proves the antenna’s capability to radiate short pulse with small distortion and maintain lower time ringing. The 2D and 3D radiation patterns including co-polarization and cross-polarization of resonance frequencies are shown in Figure 8. The antenna prototype exhibits a stable omnidirectional radiation pattern over the desired operating and resonance frequencies. At the frequency 5.1 GHz, the antenna displays a typical eight (8) shapes of radiation pattern. At higher frequency, the antenna

presents directive cross-polarization because of changing the current distribution. At higher frequency, the current does not distribute evenly because of the higher order current mode excitation which made the radiation directive. Moreover, at upper frequencies, multiple nulls can arise in current distribution which creates some back lobes. The antenna performance summary is listed in Table 1.

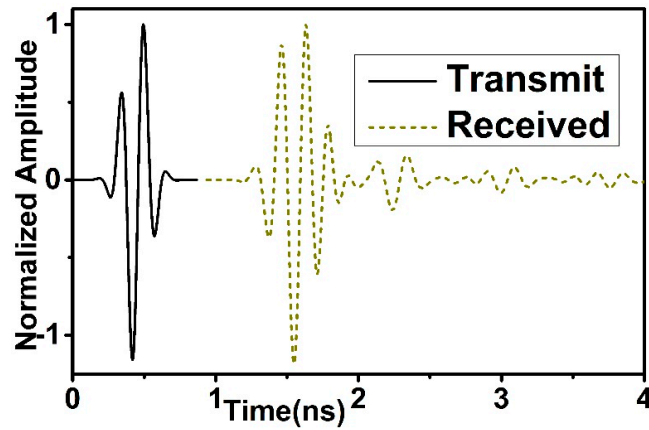
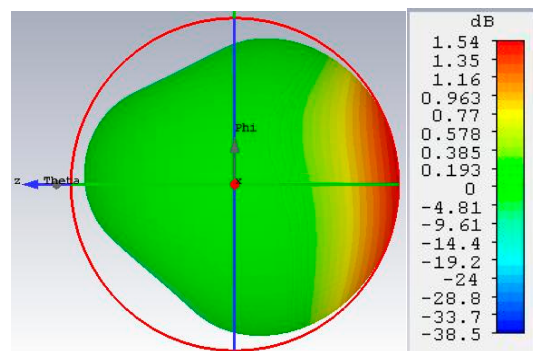
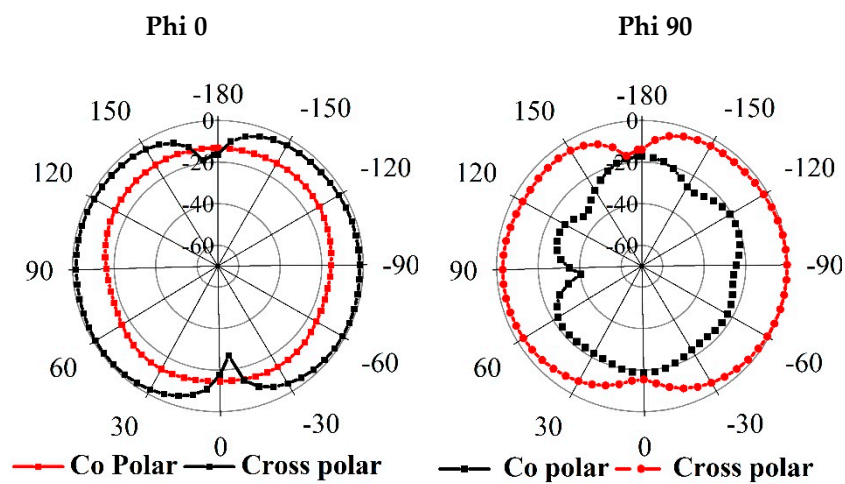


Figure 7. Transmitted and received a pulse of prototype.



(a)

Figure 8. Cont.

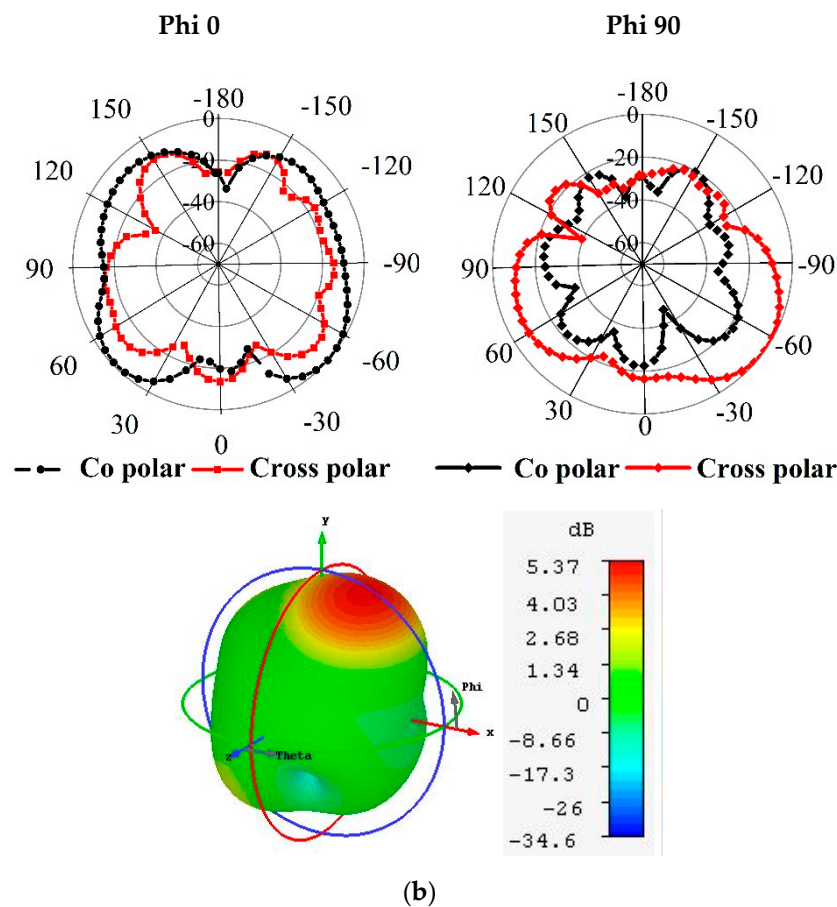


Figure 8. 2D and 3D radiation pattern of the prototype at: (a) 5.1 GHz and (b) 9.0 GHz.

Table 1. Antenna performance summary.

Properties	Antenna Performance
Dimension	$30 \times 25 \times 1.6 \text{ mm}^3$
Substrate	Rogers RT5880
Operating Bandwidth	2.7 GHz to 10.3 GHz
Fractional Bandwidth	116.92%
Gain	6.2 dBi
Efficiency	80%
Radiation Pattern	Unidirectional
Near Field Directivity (NFD)	64%

4. Imaging Performances

The imaging performance of the prototype was observed based on various parameters including analyzing the backscattering signal propagation, normalized magnitude with and without a tumor present inside the breast phantom and near field directivity (NFD). The system setup for breast phantom screening is shown in Figure 9 where nine antennas are surrounding the phantom. One prototype is acting as a transmitter, and the other eight are a receiver. The breast phantom consists of breast tissue layer and skin layer. The breast tissue layer is 8.75 cm thick, and the dielectric constant is 5.14 with a conductivity of 0.141 S/m. On the other hand, the skin layer is 2.5 mm thick, and the dielectric constant is $\epsilon_r = 38$ with 1.49 S/m conductivity. At 6 mm depth inside the phantom a 10 mm diameter tumor cell has been placed which has a high dielectric constant of 67 because of the presence of a higher amount of water content. The main aim of this system setup is to observe the change of the backscattering signal with and without the presence of a tumor cell. The normalized magnitude of two different

setups is shown in Figure 10. It is identified that the received pulse of the two-different setup has two different phases of signal propagation.

The NFD is the ratio of the radiated power through the transmitting antenna and the power received radiated power over the surface of the phantom at the receiving antenna. The calculation is done by the equation stated in [26].

$$NFD = P_f/P_T \quad (1)$$

This is the proportion of radiated power inside the phantom (P_f) and the radiated power across the surface of the phantom (P_T). Figure 11 indicates that the NFD factor for the proposed imaging setup is about 64%. That means about 64% of power is radiated through the breast tissue. The images constructed by analyzing the change of backscattering signals are shown in Figure 12. The imaging of the phantom without tumor is illustrated in Figure 12a, and the results with the presence of the tumor are presented in Figure 12b. For the higher dielectric properties of the tumor, the received signal at the point of the location of the tumor is identical than that of normal breast tissue.

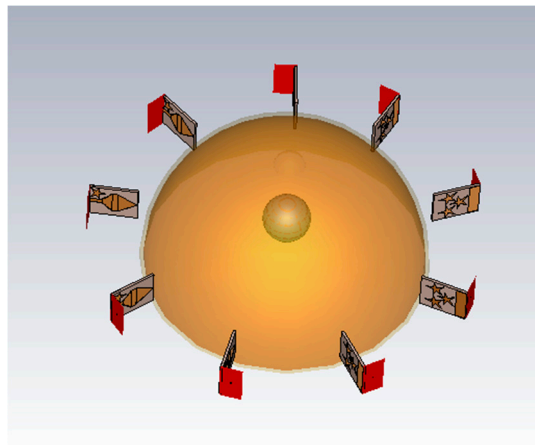


Figure 9. Proposed simulated Imaging setup with breast phantom.

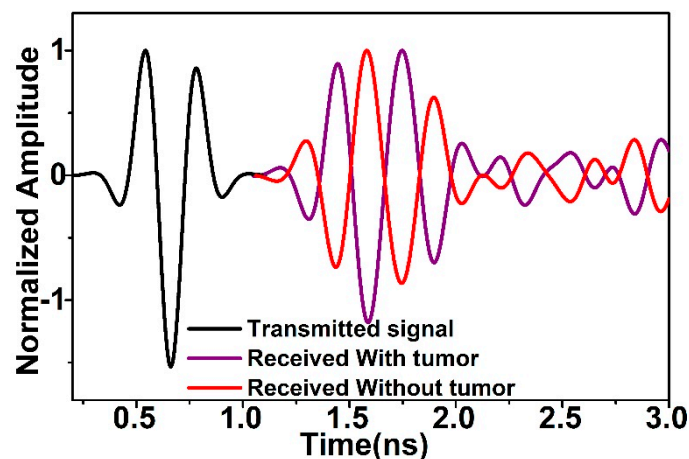


Figure 10. Normalized magnitude of the received pulse over transmitted pulse.

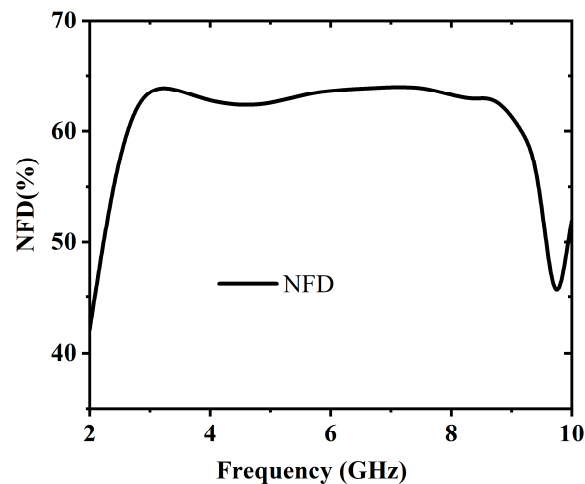


Figure 11. Near field directivity of the proposed prototype with imaging setup.

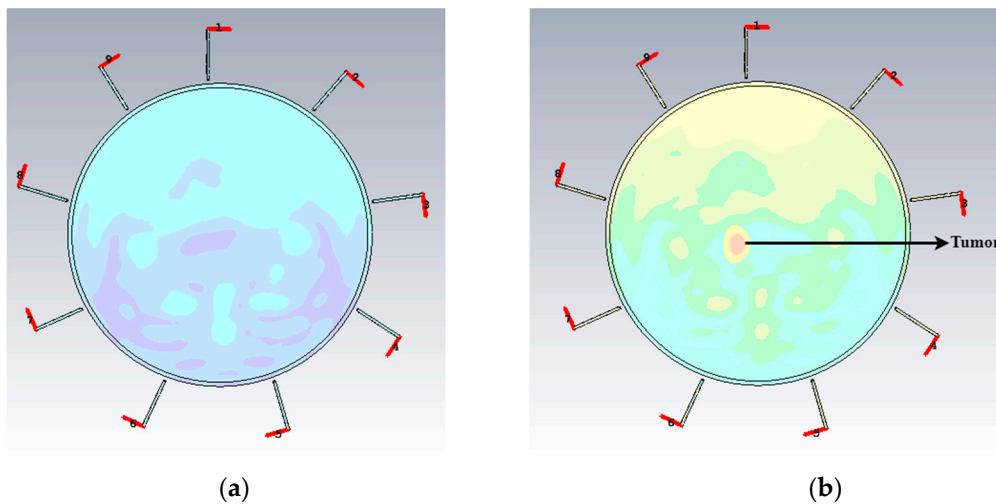


Figure 12. Images of (a) without and (b) with one tumor inside the breast phantom.

5. Conclusions

A diamond-shaped UWB antenna is proposed using asterisk-shaped parasitic elements. The use of parasitic elements on the ground and beside the feedline enhance the antenna's operating bandwidth and gain. The imaging performance of the realized antenna for a breast phantom imaging system is presented to analyze the variation of the backscattering signal and transmit-received pulses including E-field and near field directivity. The prototype achieved satisfactory fractional bandwidth over the UWB band of 116.92% (2.7 GHz to 10.3 GHz), higher gain and moderate efficiency, with a stable radiation pattern. The observation during the analysis of the numerical and measured data reveals that the antenna is suitable for UWB-based microwave imaging applications.

Author Contributions: M.Z.M., M.T.I. (Md Tarikul. Islam) and A.F.A. made substantial contributions to this research work regarding conception, design, analysis and writing the manuscript. M.S. analyzed acquired data and the results, revised the manuscript, participated in measurement and provided intellectual suggestions. U.K.A., A.F.A. and M.T.I. (Mohammad Tariqul Islam) conceptualized the proposed antenna, participated in revising the article critically for important intellectual content, and supervised the whole study.

Funding: This research was funded by Ministry of Higher Education (MOHE), Malaysia, grant number "FRGS/1/2018/TK04/UKM/01/3".

Conflicts of Interest: The authors declare no conflict of interest.

References

1. Pan, J. Medical Applications of Ultra-Wideband (UWB). Survey Paper. 2007. Available online: <https://www.cse.wustl.edu/~jain/cse574-08/ftp/uwb/> (accessed on 10 February 2019).
2. Ojaroudi, M.; Ghobadi, C.; Nourinia, J. Small square monopole antenna with inverted T-shaped notch in the ground plane for UWB application. *IEEE Antennas Wirel. Propag. Lett.* **2009**, *8*, 728–731. [[CrossRef](#)]
3. Wong, H.; So, K.K.; Gao, X. Bandwidth enhancement of a monopolar patch antenna with V-shaped slot for car-to-car and WLAN communications. *IEEE Trans. Veh. Technol.* **2016**, *65*, 1130–1136. [[CrossRef](#)]
4. Pandey, G.; Singh, H.; Bharti, P.; Meshram, M. Metamaterial-based UWB antenna. *Electron. Lett.* **2014**, *50*, 1266–1268. [[CrossRef](#)]
5. Liu, H.-W.; Yang, C.-F. Miniature hook-shaped monopole antenna for UWB applications. *Electron. Lett.* **2010**, *46*, 265–266. [[CrossRef](#)]
6. Samsuzzaman, M.; Islam, M.T. A semicircular shaped super wideband patch antenna with high bandwidth dimension ratio. *Microw. Opt. Technol. Lett.* **2015**, *57*, 445–452. [[CrossRef](#)]
7. Abbosh, A. Miniaturization of planar ultrawideband antenna via corrugation. *IEEE Antennas Wirel. Propag. Lett.* **2008**, *7*, 685–688. [[CrossRef](#)]
8. Gao, X.; Yang, H.W.; Lai, H.W.; So, K.K.; Won, H.; Xue, Q. CPW-fed slot antenna with dual band-notched characteristic for UWB application. In Proceedings of the 4th International High Speed Intelligent Communication Forum, Nanjing, China, 10–11 May 2012; pp. 1–3.
9. Lakrit, S.; Ammor, H.; Terhzaz, J.; Tribak, A. Realization and Measurements of a Miniature Square Patch Antenna for Ultra Wideband Applications. *Int. J. Microw. Opt. Technol.* **2015**, *10*, 307–313.
10. Liu, H.; Zhu, S.; Wen, P.; Xiao, X.; Che, W.; Guan, X. Flexible CPW-fed fishtail-shaped antenna for dual-band applications. *IEEE Antennas Wirel. Propag. Lett.* **2014**, *13*, 770–773.
11. Azim, R.; Islam, T.M.; Misran, N. Compact tapered-shape slot antenna for UWB applications. *IEEE Antennas Wirel. Propag. Lett.* **2011**, *10*, 1190–1193. [[CrossRef](#)]
12. Natarajan, R.; George, V.J.; Kanagasabai, M.; Shrivastav, K.A. A compact antipodal Vivaldi antenna for UWB applications. *IEEE Antennas Wirel. Propag. Lett.* **2015**, *14*, 1557–1560. [[CrossRef](#)]
13. Mahmud, M.; Islam, T.M.; Samsuzzaman, M.; Kibria, S.; Misran, N. Design and parametric investigation of directional antenna for microwave imaging application. *IET Microw. Antennas Propag.* **2016**, *11*, 770–778. [[CrossRef](#)]
14. Sharma, M.; Shrivastava, V. Printed fractal elliptical monopole antenna for UWB application. In Proceedings of the 2008 International Conference on Recent Advances in Microwave Theory and Applications, Jaipur, India, 21–24 November 2008; pp. 374–376.
15. Shaalan, A.A.; Ramadan, M. Design of a Compact Hexagonal Monopole Antenna for Ultra—Wideband Applications. *J. Infrared Millim. Terahertz Waves* **2010**, *31*, 958–968. [[CrossRef](#)]
16. Yang, B.Y.; Zhang, S.F.; Zhang, F.; Zhang, L.; Jiao, Y.C. A novel compact CPW-fed planar monopole antenna with modified stair-style ground for ultra-wideband applications. *Microw. Opt. Technol. Lett.* **2010**, *52*, 2100–2104. [[CrossRef](#)]
17. Liu, L.; Cheung, S.; Azim, R.; Islam, M.T. A compact circular-ring antenna for ultra-wideband applications. *Microw. Opt. Technol. Lett.* **2011**, *53*, 2283–2288. [[CrossRef](#)]
18. Isik, G.; Topaloglu, S. A Compact Size 4–19.1 GHz Heart Shape UWB Antenna with Triangular Patches. *Int. J. Antennas Propag.* **2013**, *2013*, 614754. [[CrossRef](#)]
19. Fear, E.C.; Hagness, S.C.; Meaney, P.M.; Okoniewski, M.; Stuchly, M.A. Enhancing breast tumor detection with near-field imaging. *IEEE Microw. Mag.* **2002**, *3*, 48–56. [[CrossRef](#)]
20. Jossinet, J.; Schmitt, M. A review of parameters for the bioelectrical characterization of breast tissue. *Ann. N. Y. Acad. Sci.* **1999**, *873*, 30–41. [[CrossRef](#)] [[PubMed](#)]
21. Islam, M.T.; Mahmud, M.Z.; Misran, N.; Takada, J.-I.; Cho, M. Microwave Breast Phantom Measurement System With Compact Side Slotted Directional Antenna. *IEEE Access* **2017**, *5*, 5321–5330. [[CrossRef](#)]
22. Belrose, J.S. The Sounds of a Spark Transmitter: Telegraphy and Telephony. *Adventures CyberSound*. 1994. Available online: <http://www.hammondmuseumofradio.org/spark.html> (accessed on 10 February 2019).

23. Torres, C.F.; Monroy, J.M.; Morales, H.L.; Pérez, R.C.; Tellez, A.C. Heart shaped monopole antenna with defected ground plane for UWB applications. In Proceedings of the 11th International Conference on Electrical Engineering, Computing Science and Automatic Control (CCE), Campeche, Mexico, 29 September–3 October 2014; pp. 1–4.
24. Mahmud, M.; Kibria, S.; Samsuzzaman, M.; Misran, N.; Islam, M.T. A New High Performance Hibiscus Petal Pattern Monopole Antenna for UWB Applications. *Appl. Comput. Electromagn. Soc. J.* **2016**, *31*, 373–380.
25. Gautam, A.K.; Yadav, S.; Kanaujia, B.K. A CPW-fed compact UWB microstrip antenna. *IEEE Antennas Wirel. Propag. Lett.* **2013**, *12*, 151–154. [[CrossRef](#)]
26. Amineh, R.K.; Trehan, A.; Nikolova, N.K. TEM horn antenna for ultra-wide band microwave breast imaging. *Prog. Electromagn. Res.* **2009**, *13*, 59–74. [[CrossRef](#)]



© 2019 by the authors. Licensee MDPI, Basel, Switzerland. This article is an open access article distributed under the terms and conditions of the Creative Commons Attribution (CC BY) license (<http://creativecommons.org/licenses/by/4.0/>).